An investigation on the propagation of 26 December 2004 tsunami waves towards the west coast of Malaysia and Thailand using a Cartesian coordinates shallow water model

Gauranga Deb Roy*† Ahmad Izani Md. Ismail*

Abstract

The tsunami of December 26, 2004, having its source at Sumatra, was very severe and caused tremendous loss of life and property along the coastal regions surrounding the Indian Ocean including the west coast of Malaysia and south west coast of Thailand. From this event it is evident that the west coast of Malaysia and Thailand is in a vulnerable region for tsunami surge due to a permanent source at Sumatra. In this paper, we propose a shallow water model in Cartesian coordinate system, for the west coast of Malaysia and Thailand. The model area includes the region between $2°N$ to $14°N$ latitudes and $91°E$ to $101.5°E$ longitudes. The generation mechanism of the 26 December 2004 tsunami is mainly the static sea floor uplift caused by abrupt slip at the India/Burma plate interface. The estimated uplift and subsidence zone is between $92°E$ to $97°E$ and $3°N$ to $10°N$ with a maximum uplift of 507 cm at the west and maximum subsidence of 474 cm at east (Kowalik et al.[6]), which is assigned as initial condition. The propagation of the tsunami wave towards the west coast of Malaysia and Thailand is simulated and the water levels along this coast are computed. Further investigations are carried out to understand different aspects of the propagation of the tsunami waves and amplitude of water levels along the coastal belt. It is found that the Cartesian coordinate shallow water model is capable of simulating different aspects of tsunami with reasonable accuracy.

Key words: Malaysia, Thailand, Shallow water model, December 26, 2004 tsunami at Sumatra, Tsunami propagation and surge.

Introduction

The tsunami of December 26, 2004, having its source at Sumatra, was very severe and caused tremendous loss of life and property along the coastal regions surrounding the Indian Ocean including west coasts of Peninsular Malaysia and Thailand (Fig. 1). From this event it is evident that the west coasts of peninsular Malaysia and Thailand are in vulnerable positions for tsunami surge due to a permanent source at Sumatra. So, it is necessary that tsunamis are studied in detail and prediction models be developed to simulate propagation and to estimate surge amplitude along the coastal belts.

*School of Mathematical Sciences, Universiti Sains Malaysia, 11800 USM, Penang, Malaysia, Fax: 60 4

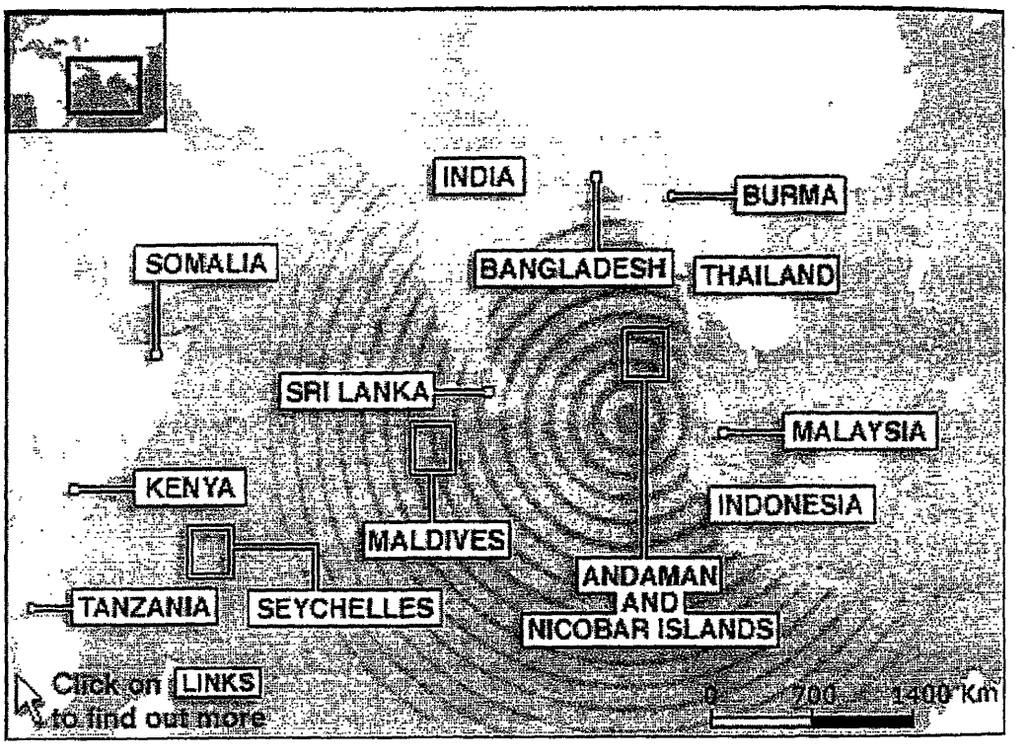

Figure 1: Major affected regions around the Indian Ocean by tsunami of 26 December 200 generated near Sumatra (Source: http://news.bbc.co.uk/1/hi/world/4126019.stm)

A tsunami is a series of very fast moving (ocean) long gravity waves generated by a rapid large-scale disturbance of seawater, especially, by large underwater earthquakes or landslides. Tsunami waves are mainly generated by the displacement of a large volume of water in a localized area where the seabed suffers a vertical displacement due to thrust-dip along a fault especially in the subduction zone (Cuypers [1]). The form of a tsunami wave changes with respect to ocean depth and coastal geometry in the shallow continental shelf. The long wave concept is based on shallow water equations in which the vertical component of momentum equation is replaced by the hydrostatic approximation. An overview of the implementation of the shallow water equations in tsunami modeling is presented in Synolaksis [10].

Kienle et al. [4] studied the propagation and run-up of tsunami waves generated by a landslide due to the eruption of the Mt. St. Augustine Volcano, Alaska in 1883. The model, based on the nonlinear shallow water equations and solved by the finite difference method, simulates run-up heights and inundation patterns. In the study of Zahibo et al. [12], numerical simulation of potential tsunamis in the Caribbean Sea is performed in the framework of the nonlinear shallow water theory. The study of Imamura and Gica [2] is based on circular-arc slip model and a subsidence model. This is developed for generation of tsunami waves due to subaqueous landslide. The model is applied to wave generation in the southern shore of Hading Bay, Flores Island, Indonesia. Titov and Gonzalez [11] developed the MOST (Method of Splitting Tsunami) Model that is capable of simulating the tsunami generation, transoceanic propagation, and inundation of dry land; the generation process is based on elastic deformation theory (Okada [7]). Kowalik and Whitmore [5] developed a model to simulate the tsunamis associated with the 1952 Kamchatka and 1986 Andreanof Islands earthquakes along the Adak of Alaska. The numerical technique was designed with uneven mesh for propagating the tsunami wave a long distance without over taxation of computer memory and time. Very recently Kowalik et al. [6] developed a global model to simulate the generation, propagation and run-up of the tsunami associated with the 26 December 2004 event throughout the globe between $80°S$ and $69°N$. They used the spherical polar shallow water model incorporating a very fine mesh resolution of one minute with about 200 million grid points.

The tsunami waves approach the coast with very high phase speeds and their amplitude increase as they reach the coastal shallow waters. In general, the coastal and island boundaries are curvilinear in nature and they are approximated along the nearest gridlines of the finite difference scheme that is used for solution purpose. In order to incorporate the coastlines and the island boundaries accurately in a numerical scheme, it is necessary to involve a very fine grid resolution along the coastal belts and offshore regions. Consideration of very fine resolution throughout the model area involves increased computer memory and CPU time in the solution process. The computing time may be reduced if one uses the nested numerical scheme where a fine mesh scheme for the coastal area is nested into a coarse mesh scheme for the whole analysis area (Johns et al. [3], Roy [8]).

After generation of tsunami at a source, the wave propagates on all sides with a very high speed. So, immediately after the generation, the people of the surrounding coastal belts must be warned about the arrival time and intensity of wave amplitude. Estimation of these can best be carried out through a numerical model. Since the time lag between the generation and inundation along a coastal belt is small because of very fast propagation, not much time is available for model simulation purpose. So any global model, which takes a long time for

6570910

Permanent position: Department of Mathematics and Natural Sciences, BRAC University, Mohakhali, Dhaka 1212, Bangladesh

simulation, is not effective for real time simulation. For this purpose a regional model may be more effective and efficient because it takes less simulation time and it is possible to incorporate fine resolution in the numerical scheme. Thus we may have more detailed information about intensity and other aspects of the tsunami around the region of interest.

The west coast of southern Thailand and Peninsular Malaysia is facing towards the Sumatra Island where there is a permanent tsunami source (Fig. 2). Penang Island in Malaysia and the Phuket in Thailand were lashed by high tsunami surges due to the source at Sumatra on 26 December 2004. Thus Penang Island and Phuket appear to be vulnerable for high surge due to source at Sumatra. So attention should be given on prediction of tsunami along the coastal belt of Malaysia and southern Thailand. From a literature survey, it is found that not much work has been done on tsunami modeling for this region.

In the present study a Cartesian coordinate shallow water model has been applied to simulate the propagation of tsunami that originated at Sumatra on 26 December 2004 and to estimate the water level along the west coasts of Peninsular Malaysia and Thailand (Fig. 2). The analysis area is a rectangular region approximately between $2°N$, $14°N$ and $101.5°E$, $91°E$. The model area includes well the tsunami source region associated with 26 December 2004 event near Sumatra Island. A rectangular grid system is incorporated by considering the lines parallel to x-axis and y-axis respectively. An explicit finite difference scheme is used in solving the shallow water equations using initial and boundary conditions to simulate the propagation of the tsunami wave towards the coast of Malaysia and Thailand and to estimate the water levels at different locations including Penang Island and Phuket.

2 Shallow Water Model

2.1 Depth averaged shallow water equations

A system of rectangular Cartesian coordinates is used in which the origin, O, is in the undisturbed sea surface (MSL), x-axis and y-axis are on MSL and Oz is directed vertically upwards. We consider the displaced position of the free surface as $z = (x, y, t)$ and the sea floor as $z = -h(x, y)$ so that, the total depth of the fluid layer is $\zeta + h$. The vertically integrated shallow water equations are

$$\frac{\partial \zeta}{\partial t} + \frac{\partial}{\partial x}[(\zeta + h)u] + \frac{\partial}{\partial y}[(\zeta + h)v] = 0 \tag{1}$$

$$\frac{\partial u}{\partial t} + u\frac{\partial u}{\partial x} + v\frac{\partial u}{\partial y} - fv = -g\frac{\partial \zeta}{\partial x} + \frac{T_x - F_x}{\rho(\zeta + h)} \tag{2}$$

$$\frac{\partial v}{\partial t} + u\frac{\partial v}{\partial x} + v\frac{\partial v}{\partial y} + fu = -g\frac{\partial \zeta}{\partial y} + \frac{T_y - F_y}{\rho(\zeta + h)} \tag{3}$$

where

u, v = velocity components of sea water in x and y directions, m s^{-1}

f = Coriolis parameter, $s^{-1} = 2\Omega \sin\varphi$

Ω = angular speed of earth, rad s^{-1}

φ = latitude of a location in the analysis area, rad

g = gravity acceleration, m s^{-2}

T_x, T_y = components of wind stress, N m^{-2}

F_x,F_y = components of bottom friction, N m^{-2}

h = ocean depth from the mean sea level, m.

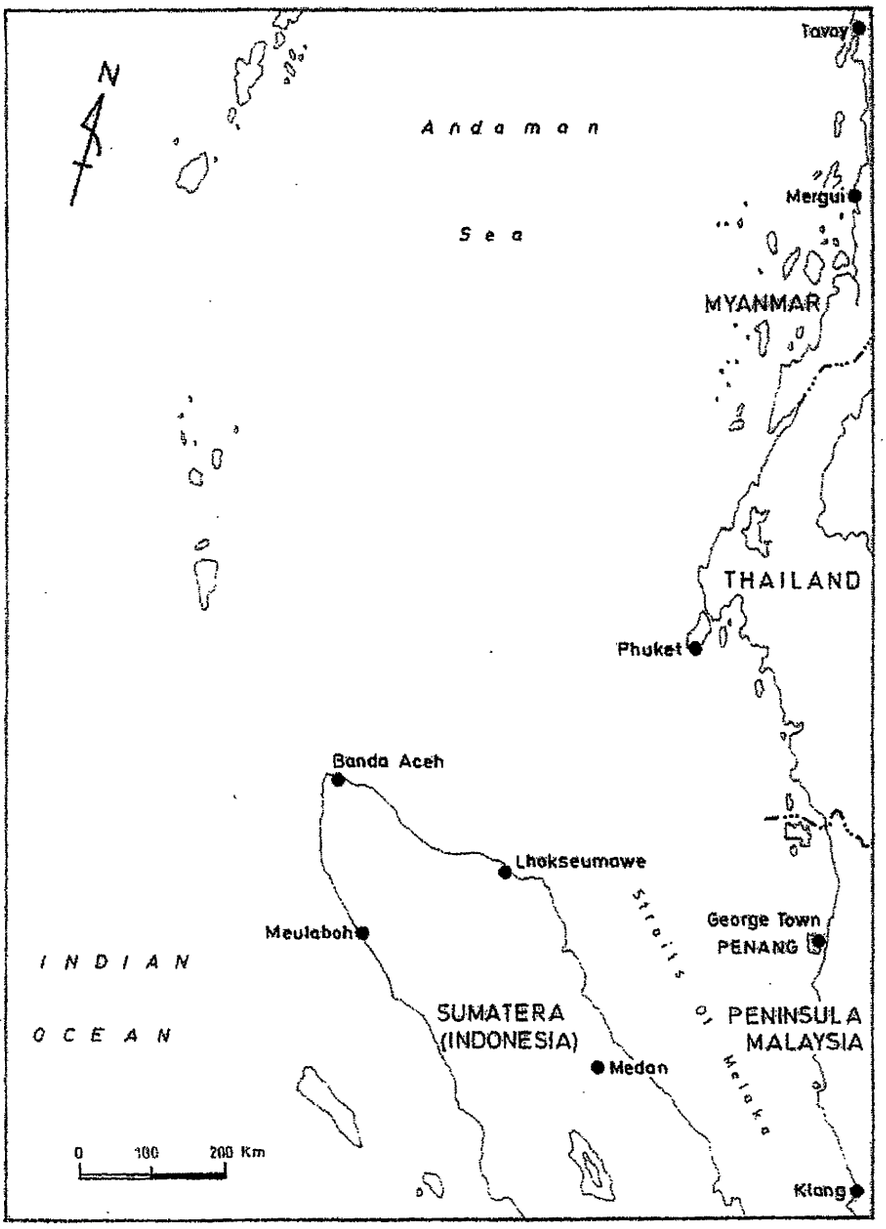

Figure 2: Map of the area included in the model

Since our study is on simulation of tsunami only, we neglect the wind stress terms T_x and T_y. On the other hand, the parameterization of the bottom stress is done by the depth averaged velocity components:

$$F_x = \rho C_f u \left(u^2 + v^2\right)^{1/2} \quad \text{and} \quad F_y = \rho C_f v \left(u^2 + v^2\right)^{1/2} \tag{4}$$

where C_f = the friction coefficient, ρ = water density, kg m^{-3}.

For numerical treatment it is convenient to express the Eqs. (2) & (3) in the flux form by using the Eq. (1). Using the parameterization formulas (4), the Eqs. (1) - (3) may be expressed as

$$\frac{\partial \zeta}{\partial t} + \frac{\partial \tilde{u}}{\partial x} + \frac{\partial \tilde{v}}{\partial y} = 0 \tag{5}$$

$$\frac{\partial \tilde{u}}{\partial t} + \frac{\partial (u\tilde{u})}{\partial x} + \frac{\partial (v\tilde{u})}{\partial y} - f\tilde{v} = -g(\zeta + h)\frac{\partial \zeta}{\partial x} - \frac{C_f \tilde{u}\left(u^2 + v^2\right)^{1/2}}{\zeta + h} \tag{6}$$

$$\frac{\partial \tilde{v}}{\partial t} + \frac{\partial (u\tilde{v})}{\partial x} + \frac{\partial (v\tilde{v})}{\partial y} + f\tilde{u} = -g(\zeta + h)\frac{\partial \zeta}{\partial y} - \frac{C_f \tilde{v}\left(u^2 + v^2\right)^{1/2}}{\zeta + h} \tag{7}$$

where, $(\tilde{u}, \tilde{v}) = (\zeta + h)(u, v)$

In the bottom stress terms of (6) & (7), u and v have been replaced by $\tilde{u}$ and $\tilde{v}$ in order to solve the equations in a semi-implicit manner.

2.2 Boundary Conditions

Other than the west coast of Peninsular Malaysia and Thailand, the boundaries are considered as straight lines in the sea. The southern and northern open sea boundaries lie parallel to x-axis and the western open sea boundary lies parallel to y-axis. The radiation boundary conditions for the southern, northern and western open sea boundaries, due to Roy [8], are

$$u - (g/h)^{1/2}\zeta = 0 \quad \text{at the west open boundary; parallel to } y\text{-axis} \tag{8}$$

$$v + (g/h)^{1/2}\zeta = 0 \quad \text{at the south open boundary; along } x\text{-axis} \tag{9}$$

$$v - (g/h)^{1/2}\zeta = 0 \quad \text{at the north open boundary; parallel } x\text{-axis} \tag{10}$$

This type of boundary condition allows the disturbance, generated within the model area, to go out through the open boundary. The coastal belts of the main land and islands are the closed boundaries where the normal components of the current are taken as zero.

2.3 Initial condition (Tsunami source generation)

The generation mechanism of the 26 December 2004 tsunami was mainly a static sea floor uplift caused by an abrupt slip at the India/Burma plate interface. A detailed description of the estimation of the extent of the earthquake rapture as well as the maximum uplift and subsidence of the seabed is given in Kowalik et al. [6] and this estimation is based on Okada [7]. From the deformation contour, it is seen that the estimated uplift and subsidence zone is between $92°E$ to 97°E and 2°N to 10°N with a maximum uplift of 507 cm at the west and maximum subsidence of 474 cm at the east (Fig. 4 of Kowalik et al. [6]). The uplift to subsidence is approximately from west to east relative to the west coasts of the Malaysian

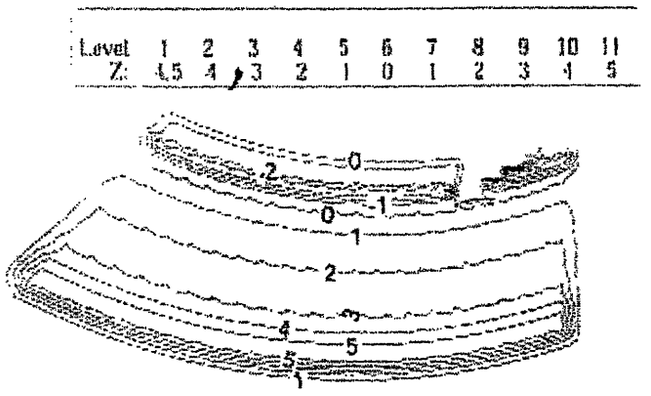

Figure 3: Tsunami source shown as contours of sea surface elevation and subsidence

Peninsula and Thailand. In this study, the disturbance in the form of uplift and down-drop of sea surface is assigned as the initial condition in the model with a maximum up lift of 5 m to maximum down-drop of 4.75 m. The source, in the form of contour, is shown in Fig. 3 and the vertical cross-section of the source along the 154th grid line parallel to x-axis is shown in Fig. (5a). This grid line is passing through the Phuket region in south west Thailand. In all other regions the initial sea surface elevations are taken as zero. Also the initial x and y components of velocity are taken as zero throughout the model area.

3 Grid Generation and Boundary Approximation

We generate the rectangular grid system in the analysis area using a set of equidistant straight lines parallel to x-axis and a set of equidistant straight lines parallel to y-axis. The space between any two consecutive gridlines parallel to y-axis is Δx and that between any two consecutive gridlines parallel to x-axis is Δy. Let there are M gridlines parallel to y-axis and N gridlines parallel to x-axis. So, there are$M$ grid points in x-direction and N grid points in y-direction and the total number of grid points are $M \times N$. We define the discrete$M \times N$ grid points (x_i, y_j) in the domain by

$$x_i = (i-1)\Delta x, \quad i = 1, 2, 3, \ldots M \tag{11}$$

$$y_j = (j-1)\Delta y, \quad j = 1, 2, 3, \ldots N \tag{12}$$

The sequence discrete time instants is given by

$$t_k = k\Delta t \quad k = 1, 2, 3, \ldots \tag{13}$$

To solve the model equations we use a conditionally stable semi-implicit finite difference method using staggered grid (Fig. 4) in which there are three distinct types of computational points (x_i, y_j) . With i even and j odd, the point is a ζ-point at which ζ is computed from the continuity equation. If i is odd and j is odd, the point is a u-point at which u is computed from the x-component of momentum equation. If i is even and j is even, the point is a v-point

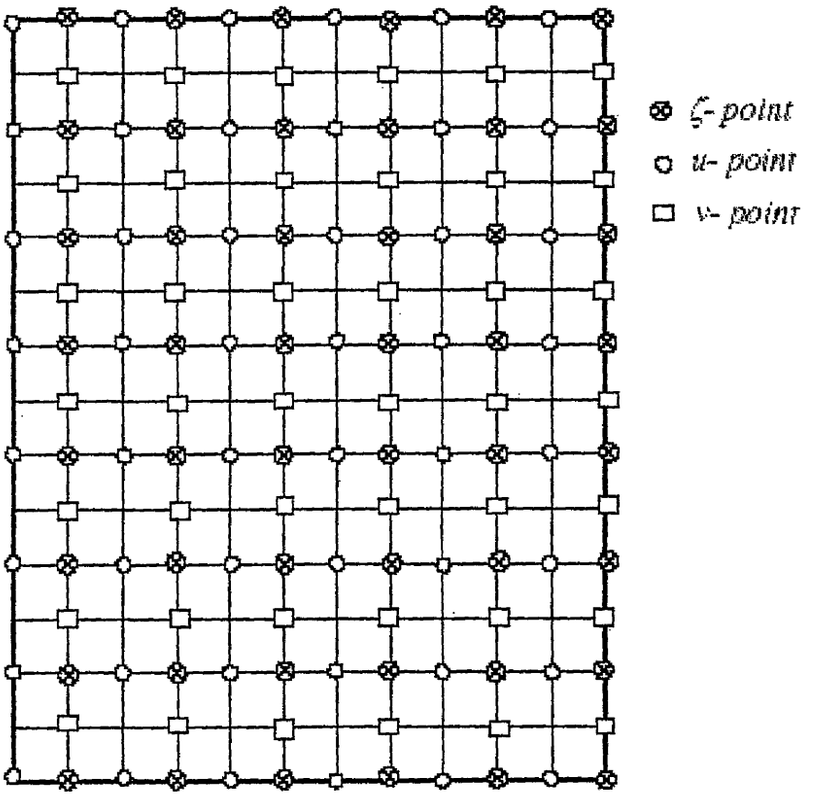

Figure 4: Staggered grid system that is used in the numerical scheme

at which v is computed from the y-component of momentum equation. We choose$M$ to be even so that at the open boundary, parallel to y-axis, there are ζ-points and v-points. We choose N to be odd, thus ensuring ζ-points and u-points along two open boundaries parallel to x-axis. In the numerical scheme the coastal and island boundaries are approximated by continuous segments either along the nearest y-directed odd gridline (i= odd) or along the nearest x-directed even grid line (j= even). Thus each boundary is represented by such a stair step that, at each segment there exists only that component of velocity which is normal to the segment. This is done in order to ensure the vanishing of the normal component of velocity at each boundary segment.

4 Discretization and Finite Difference Scheme

The governing equations are discretized by finite differences (forward in time and central in space) and are solved by a conditionally stable semi-implicit method. For the purpose of discretization we use the notations as follows: For any dependent variable $\chi(x, y, t)$,

$$\chi(x_i, y_j, t_k) = \chi_{ij}^k$$

$$\frac{1}{2}(\chi_{i+1j}^k + \chi_{i-1j}^k) = \overline{\chi_{ij}^k}^x$$

$$\frac{1}{2}(\chi_{ij+1}^k + \chi_{ij-1}^k) = \overline{\chi_{ij}^k}^y$$

$$\frac{1}{4}(\chi_{i+1j}^k + \chi_{i-1j}^k + \chi_{ij+1}^k + \chi_{ij-1}^k) = \overline{\chi_{ij}^k}^{xy}$$

The discretized form of Eq. (5) is

$$\frac{\zeta_{ij}^{k+1} - \zeta_{ij}^k}{\Delta t} + \frac{\tilde{u}_{i+1j}^k - \tilde{u}_{i-1j}^k}{2\Delta x} + \frac{\tilde{v}_{ij+1}^k - \tilde{v}_{ij-1}^k}{2\Delta y} = 0 \tag{14}$$

from which we compute ζ_{ij}^{k+1} for $i = 2, 4, 6, \ldots, M-2$ and $j = 3, 5, 7, \ldots, N-2$. The boundary condition (8) is discretized as

$$u_{M-1j}^k - (g/h_{M-1j})^{1/2}\frac{1}{2}\left(\zeta_{M-2j}^{k+1} + \zeta_{Mj}^{k+1}\right) = 0 \tag{15}$$

from which we compute ζ_{Mj}^{k+1} for $j = 1, 3, 5, \ldots, N$. The boundary condition (9) is discretized as

$$v_{i2}^k + (g/h_{i2})^{1/2}\frac{1}{2}\left(\zeta_{i1}^{k+1} + \zeta_{i3}^{k+1}\right) = 0 \tag{16}$$

from which we compute ζ_{i1}^{k+1} for $i = 2, 4, 6, \ldots, M-2$. The boundary condition (10) is discretized as

$$v_{iN-1}^k - (g/h_{iN-1})^{1/2}\frac{1}{2}\left(\zeta_{iN-2}^{k+1} + \zeta_{iN}^{k+1}\right) = 0 \tag{17}$$

from which we compute ζ_{iN}^{k+1} for $i = 2, 4, 6, \ldots, M-2$. The discretized form of Eq. (6) is

$$\frac{\tilde{u}_{ij}^{k+1} - \tilde{u}_{ij}^k}{\Delta t} + \frac{(u\tilde{u})_{i+2j}^k - (u\tilde{u})_{i-2j}^k}{4\Delta x} + \frac{(\overline{v}^x\overline{\tilde{u}}^y)_{ij+1}^k - (\overline{v}^x\overline{\tilde{u}}^y)_{ij-1}^k}{2\Delta y} - f\overline{\tilde{v}_{ij}}^{xy}$$

$$= -g(\overline{\zeta_{ij}^{k+1}}^x + h_{ij})\frac{\zeta_{i+1j}^{k+1} - \zeta_{i-1j}^{k+1}}{2\Delta x} - \frac{C_f\tilde{u}_{ij}^{k+1}\left((u_{ij}^k)^2 + (\overline{v_{ij}^k}^{xy})^2\right)^{1/2}}{\overline{\zeta_{ij}^{k+1}}^x + h_{ij}} \tag{18}$$

from which we compute $\tilde{u}_{ij}^{k+1}$ for $i = 3, 5, 7, \ldots, M-1$ and $j = 3, 5, 7, \ldots, N-2$. For $i = M$ - 1, the term $(u\tilde{u})_{i+2j}^{k}$ is evaluated by a one-sided formula. Note that in the last term $\tilde{u}_{ij}^{k+1}$ is in advanced time level and this ensures a semi-implicit nature of the numerical method. Similarly, the discretized form of Eq. (7) is

$$\frac{\tilde{v}_{ij}^{k+1} - \tilde{v}_{ij}^{k}}{\Delta t} + \frac{(\overline{u}^{y}\overline{\tilde{v}}^{x})_{i+1j}^{k} - (\overline{u}^{y}\overline{\tilde{v}}^{x})_{i-1j}^{k}}{2\Delta x} + \frac{(v\tilde{v})_{ij+2}^{k} - (v\tilde{v})_{ij-2}^{k}}{4\Delta y} + f\overline{\tilde{u}_{ij}}^{xy}$$
$$= -g(\overline{\zeta_{ij}^{k+1}}^{y} + h_{ij})\frac{\zeta_{ij+1}^{k+1} - \zeta_{ij-1}^{k+1}}{2\Delta y} - \frac{C_f \tilde{v}_{ij}^{k+1}\left((\overline{u_{ij}^{k}}^{xy})^2 + (v_{ij}^{k})^2\right)^{1/2}}{\overline{\zeta_{ij}^{k+1}}^{y} + h_{ij}} \tag{19}$$

from which we compute $\tilde{v}_{ij}^{k+1}$ for $i = 2, 4, 6, \ldots, M-2$ and $j = 2, 4, 6, \ldots, N-1$. For $j = 2$, the term $(v\tilde{v})_{ij-2}^{k}$ and for $j = N-1$ the term $(v\tilde{v})_{ij+2}^{k}$ are evaluated by one-sided formulas. As before, in the last term $\tilde{v}_{ij}^{k+1}$ is in advanced time level and this ensures a semi-implicit nature of the numerical method.

5 Model Data Set-up

The origin of the Cartesian coordinate system is at O (3.125°E, 101.5°N), x-axis is directed towards west at an angle 15° with the latitude line through O and the y-axis is directed towards north inclined at an angle 15° with the longitude line through O (Fig. 2). The grid size of the rectangular mesh is given by $\Delta x = \Delta y = 4$ km and number of grids in x-direction and y-direction are respectively M =230 and N = 319 so that there are 73370 grid points in the computational domain. The time step Δt of the numerical scheme is taken as 10 seconds and this satisfies the CFL criterion and thus ensures the numerical stability of the numerical scheme. The value of the friction coefficient C_f in each of Eqs.(6, 7) is taken as 0.0033 through out the model area. These depth data for the model area are collected from the Admiralty bathymetric charts.

6 Results and Discussions

The set of equations (5)-(7) along with the boundary conditions (8)-(10) and initial conditions described above are solved using a finite difference scheme. The finite difference form of those equations and boundary conditions are shown in (14)-(19). In computing the water level due to tsunami wave along the coastal belt, we have assumed a solid wall boundary along which the normal component of velocity is taken as zero and the initial conditions are ensured as mentioned in section 2.3.

6.1 Propagation of tsunami towards the Penang Island and Phuket

The propagation of the tsunami wave, which is originated at the source in the form sea level rise and subsidence (Fig. 3), has been studied. The propagation of the disturbance along the 154th gridline, parallel to x-axis, starting from the western open boundary to the coast of Phuket (230th to 49th grid points) is shown in Fig. 5. The figure shows the pattern of disturbance at 0 min, 60 min, 90 min and 103 min (time of maximum water level at the coast of west Phuket) along the 154th grid line. At 0 min the elevation/subsidence pattern

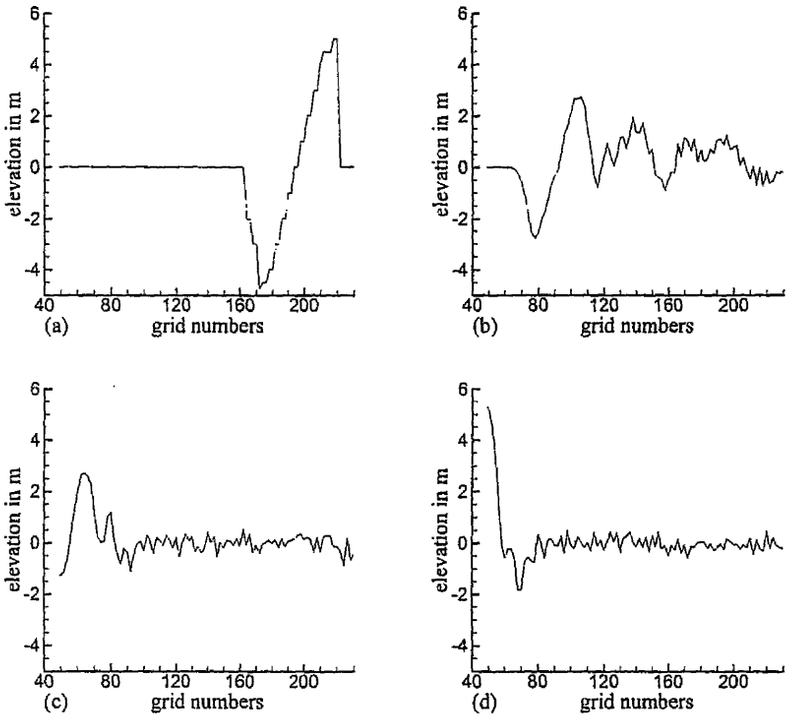

Figure 5: Disturbance pattern at different instants of time along the 154th grid line parallel to x-axis; (a) at 0 min (source), (b) at 60 min, (c) at 90 min, (d) at 103 min (time of high surge)

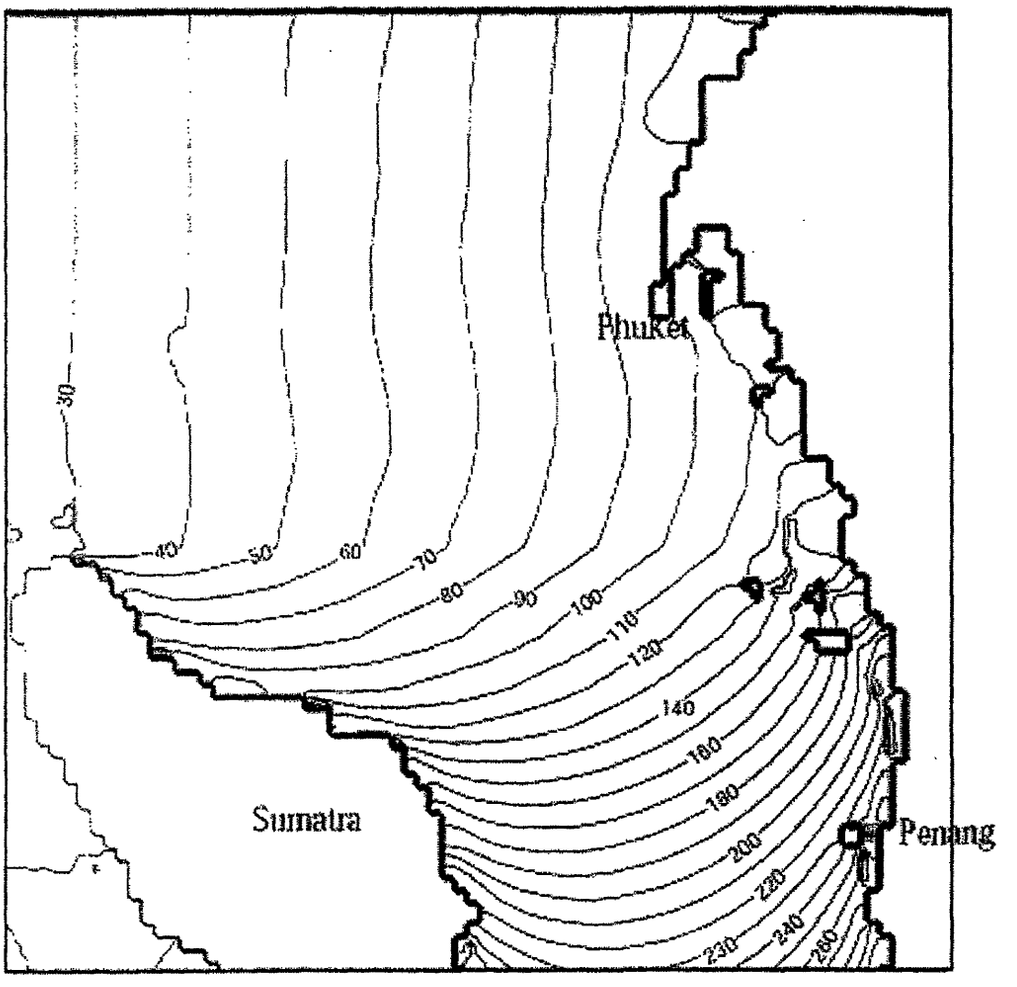

Figure 6: Contour showing tsunami propagation time in minutes; sea level rise of 0.1 m is considered as the arrival of tsunami

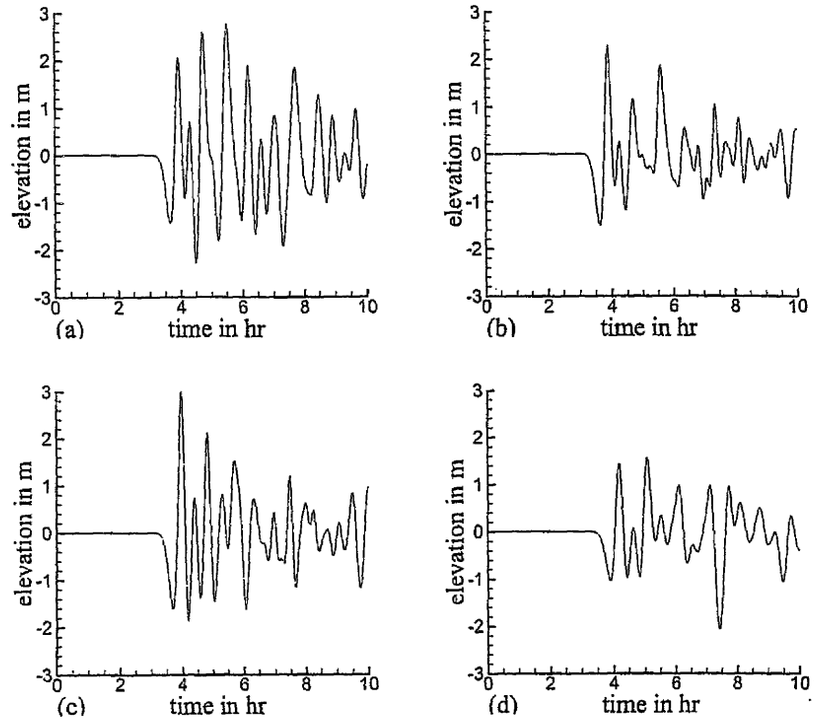

Figure 7: Time series of computed elevation at coastal locations of Penang Island associated with tsunami source at Sumatra on 26 December, 2004 (subsidence to uplift relative to west coast of Malaysia and Thailand): (a) Batu Ferringhi (north), (b) Pantai Aceh (north-west), (c) Pasir Panjang (south-west), (d) south Penang

(Fig. 5a) is of the source itself. Considering the time of first sea surface rise as time of arrival of tsunami, we see that the tsunami wave reaches the grid locations 92, 54 and 49 at approximately 60 min, 90 min and 103 min respectively (Fig.5). Thus the tsunami gradually propagates towards Phuket with time and attains a maximum of 5.4 m at the coast at 103 min (Fig. 5d). The propagation of tsunami is also shown in the form of contour plot of time, in minutes, for attaining +0.1 m sea level rise at each grid point (Fig. 6). Thus considering the 0.1 m sea level rise as the arrival of tsunami, it is seen that after initiating the source the disturbance propagates gradually towards the coast. The arrival time of tsunami at Phuket and Penang are approximately 100 min and 230 min. So tsunami wave have reached Phuket much earlier than Penang and the propagation slows down at the Malacca straits because of shallow water along this Strait. This is consistent with the fact that long wave speed reduces in shallow water.

6.2 Computed water levels along the Penang Island and Phuket

The computed water levels at different locations of the coastal belt of Penang Island are stored at an interval of 30 seconds. Figure 7 depicts the time series of water levels at four locations on the north, west and south coasts of Penang Island in Malaysia. At Batu Ferringhi (north coast) the maximum elevation is approximately 2.8 m (Fig. 7a). It is important to note that

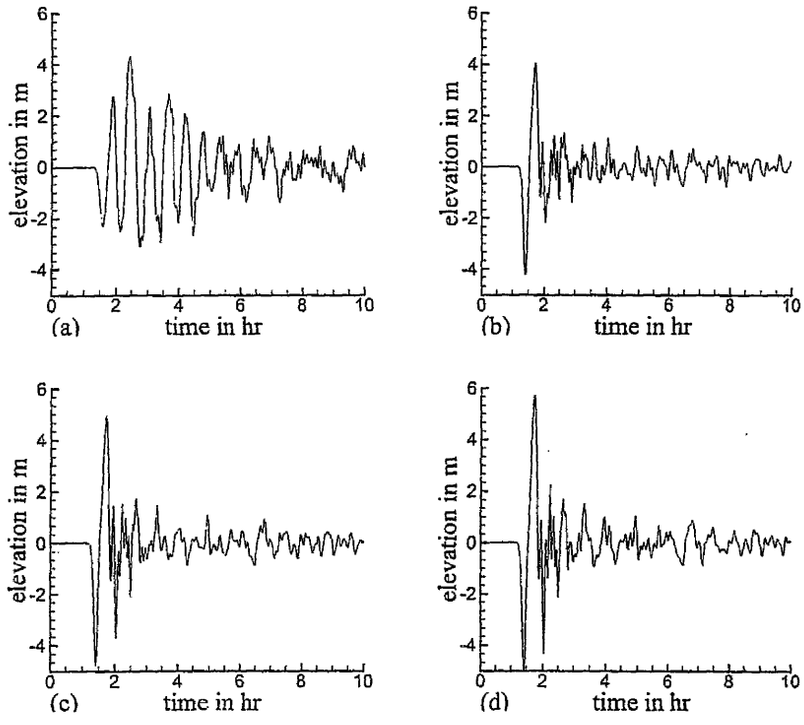

Figure 8: Time series of computed elevation at coastal locations of Phuket associated with tsunami source at Sumatra on 26 December, 2004 (subsidence to uplift relative to west coast of Malaysia and Thailand): (a) East Phuket, (b) South Phuket, (c) South-west Phuket, (d) North-west Phuket

at approximately 3 hrs after the generation of tsunami at the source, instead of increasing, the water level starts decreasing as the response to the tsunami source and reaches a minimum level of -1.4 m. Then the water level increases continuously to reach a level of 2.0 m at 3 hrs 30 min before going down again. The water level oscillates and this oscillation continues for several hours. Gaze records of tsunami also show the same pattern; for example deep ocean BPR (bottom pressure recorder) records, of water level at different locations in the Pacific Ocean during the 1996 Andreanov earthquake, show that oscillation continues for long time (see Fig. 3 of Titov and Gonzalez [11]). However, we could not verify the computed results with any tide gaze record. At the location Pantai Aceh (north-west) the maximum elevation is approximately 2.5 m (Fig. 7b). Near Pasir Panjang (south-west) the maximum elevation is found to be 3.0 m (Fig. 7c). At the south coast the the maximum surge level is estimated to be 1.6 m. The computed results show that the west coast of Penang Island is vulnerable to a stronger tsunami surge. Figure 8 depicts similar results for the Phuket region in south west Thailand. At the east coast of Phuket, the maximum water level is 4.2 m and the water level continues to oscillate for long time (Fig. 8a). The water level goes below the MSL to about -1.4 m before the arrival of the positive surge of tsunami. At the south coast of Phuket the time series begins with a depression of - 4 m and the maximum water level reaches up to 4 m and the oscillation continues with low amplitudes (Fig. 8b). At the south-west and north-west of Phuket the maximum water levels are 5 m and 5.8 m respectively (Fig. 8c, d). We have seen that the tsunami oscillation at each coastal location begins with the subsidence of water level instead of rising up as the response of tsunami source (Figs. 7, 8). We will now investigate the reason of this typical oscillation as the response of tsunami source. Among many features of tsunami as recorded near a coast, two have been frequently (but not always) reported (Shepard [9]). One feature is that the arrival of tsunami is often preceded by the withdrawal of water from the beaches, and the other is that the first crest may not be the largest. The computed results also show the withdrawal of water from the coastal region before arrival of high surge (Figs. 7, 8). It is mentioned earlier that, relative to the west coast of Malaysian Peninsula and Thailand the tsunami source is in the form of subsidence to uplift. To identify whether this relative position of the tsunami source is responsible for withdrawal of water from the coastal belt before arrival of tsunami surge, two experiments are undertaken to study the response of two different types of tsunami sources. Firstly, the source, situated at the same position, consists of only sea level rise with a maximum of 5 m without any subsidence. Since the region of subsidence is now replaced by mean sea level, the intensity of response has been reduced considerably (Fig. 9, 10). But the interesting feature is with the nature of the response that is occurring along the coastal belt. At each location the initial response of the source is in the form of sea level rise, instead of fall as in the earlier case. This means that in this case the arrival of tsunami is not preceded by the withdrawal of water from the coastal belt. So the nature of the response depends upon the nature of the source.

To confirm this idea second experiment is carried out with a source, at the same location but with the positions of elevation and subsidence reversed. In this experiment relative to west coast of Malaysian Peninsula and Thailand, the source is in the form of sea level rise to subsidence. Results of this experiment show that, at each location, the tsunami surge is not preceded by withdrawal of water from the coast (Figs. 11, 12). From these experiments it is evident that, the withdrawal of water from a coastal belt before arrival of tsunami depends upon the nature of the source. In fact, according to the conservation principle, the region of subsidence at the source must be filled up with water from the surroundings; this is why the withdrawal of water from the surroundings of the subsidence zone takes place before the

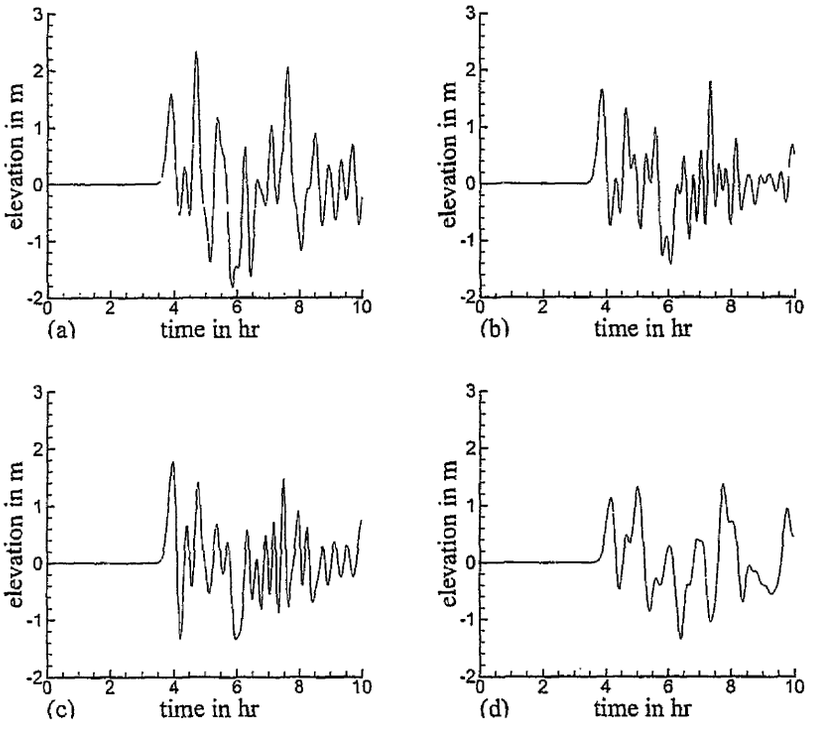

Figure 9: Same as Fig. 7, except that from the source the subsidence has been excluded (only uplift): (a) Batu Ferringhi (north), (b) Pantai Aceh (north-west), (c) Pasir Panjang (south-west), (d) south Penang

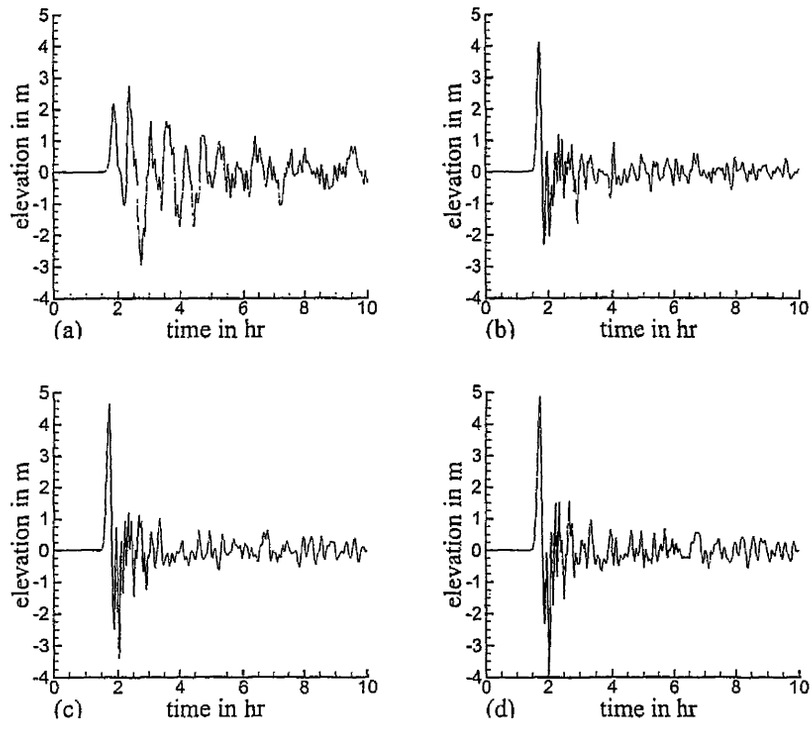

Figure 10: Same as Fig. 8, except that from the source the subsidence has been excluded (only uplift): (a) East Phuket, (b) South Phuket, (c) South-west Phuket, (d) North-west Phuket

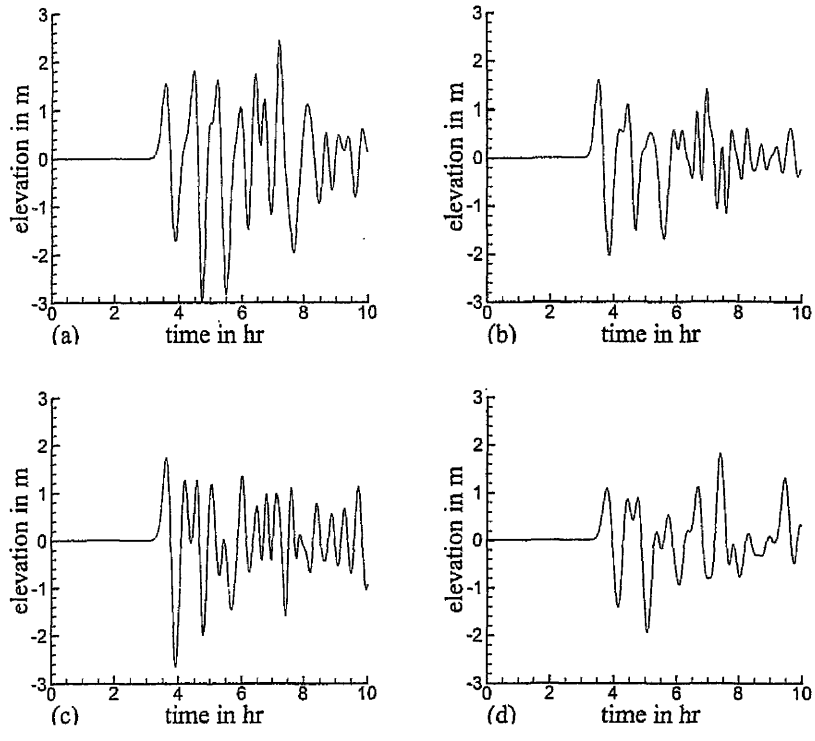

Figure 11: Same as Fig. 7, except that the source has been reversed (uplift to subsidence relative to west coast of Malaysia and Thailand): (a) Batu Ferringhi (north), (b) Pantai Aceh (north-west), (c) Pasir Panjang (south-west), (d) south Penang

arrival of the actual surge of tsunami.

The computed peak elevation surrounding Phuket can be seen from the contour plot of maximum elevation in Fig. 13. From the contour plot it is evident that the surge amplitude is increasing along the coast from south to north and the surge amplitude is ranging from 4 m to 6 m in Phuket.

6.3 Verification of computed results

Finally, a post tsunami survey report on run-up heights at different locations of Penang Island, along with the computed water level, is shown in Table 1. It should be noted that the computed water level cannot be compared with observed run-up height data, although keeping all other conditions the same, the run-up height is directly proportional to the water level at the shore line. For the same water level at two different locations the run-up height will in general be different because of the different pattern of the onshore region. For example two locations of Pasir Panjang are very close to each other as their latitudes and longitudes are almost same. The computed water levels are also same (about 3.0 m); but the run-up heights are 8.5 m and 4.2 m respectively. According to the survey report, at the first location, the tsunami wave jumped over a slope masonry wall and the roof of the house behind; whereas in the second location the inundation was blocked by a hill. A consistency between the computed water level and the run-up height at each location may be observed from the table.

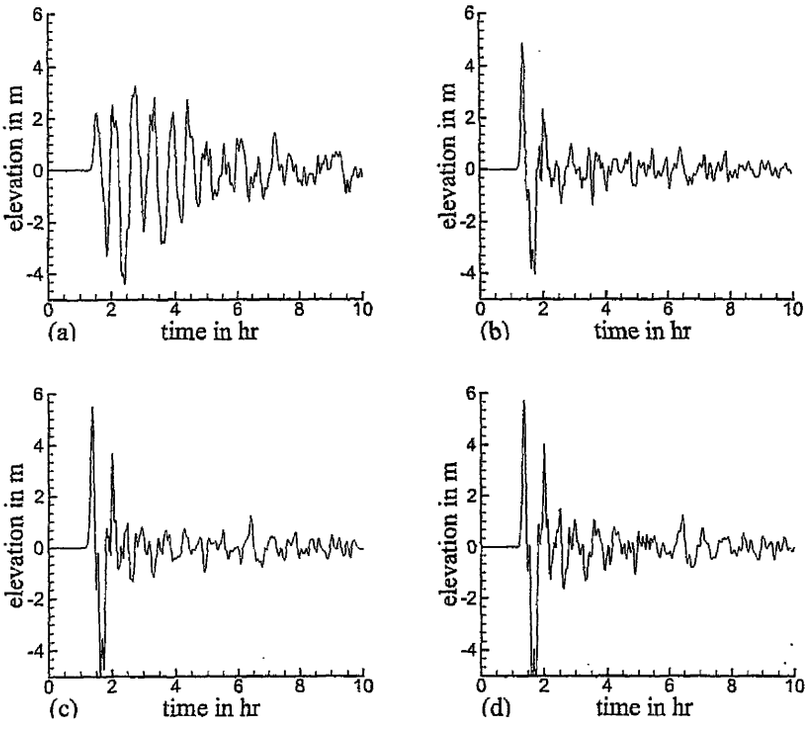

Figure 12: Same as Fig. 8, except that the source has been reversed (uplift to subsidence relative to west coast of Malaysia and Thailand): (a) East Phuket, (b) South Phuket, (c) South-west Phuket, (d) North-west Phuket

Table 1: Observed run-up heights and computed water levels above MSL at different locations in Penang island

Location name	latitude	longitude	run-up height (m)	Computed water level (m)
1	2	3	4	5
Batu Ferringhi (Teluk Bayu)	5° 28.26′	100° 14.63′	3.46	2.8
Batu Ferringhi (Miami beach)	5° 28.67′	100° 16.07′	4.00	2.8
Pasir Panjang	5° 18′	100° 11.09′	8.50	3.0
Pasir Panjang	5° 17.99′	100° 11.1′	4.20	3.0

Source: This survey was conducted by a team headed by Prof. S. B. Yoon, Hanayng University, Korea.

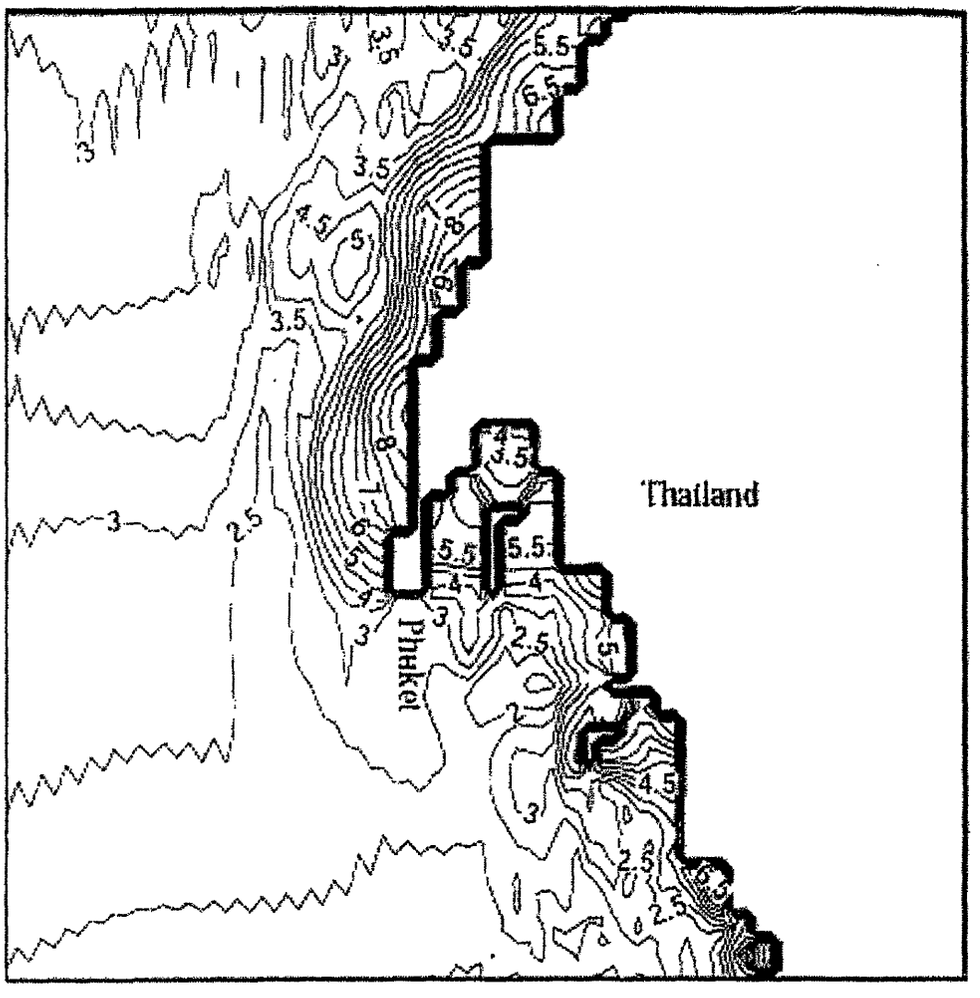

Figure 13: Contour of maximum water levels around Phuket

Table 2: Estimated and computed water levels above MSL at different locations in Penang island

Location name	Estimated water level (m)	Computed water level (m)
Batu Ferringhi (north Penang)	3.0	2.8
Tanjong Bunga (north Penang)	3.0	2.8
Kuala Pulau Betong (south Penang)	1.9	1.6

Source: This survey was conducted by the authors.

The authors of this paper made a survey to estimate the water level at different locations of Penang Island along with time of arrival of high wave along the coastal belt. The authors' effort was to estimate the maximum water level (not run-up height) above the MSL at some suitable locations where water could flow over the shore without major obstruction and the levels of water were available from spots on walls or trees and based upon the opinion of the local witness. It should be noted that the tsunami wave amplitude may be modified by tidal condition and surface waves. Table 2 shows the computed and estimated water levels at three locations. The computed water levels are in good agreement with the corresponding estimated levels. The arrival of high surge at different locations of Penang Island was between 1310 and 1330 (Malaysian time) and rapture time was 0859 (Malaysian time). Hence the propagation time was between 4 hr 11 min and 4 hr 31 min. It may be seen from Fig. 6 that the arrival time of tsunami at Penang Island is 230 min or 3 hr 50 min, which the time of attaining water level of 0.1 m only. If we consider that it takes at least 15 min to attain the highest level, then the arrival time of high surge at Penang Island is approximately 4 hr 5 min. So the agreement between the observed and computed time of arrival is satisfactory.

7 Conclusion

In this paper we have developed and applied a shallow water model in Cartesian coordinates to simulate the effects of the December 26, 2004 tsunami along the west coast of Malaysia and Thailand. It is found that the model, which is solved by an explicit finite difference method, is able to simulate the propagation of tsunami wave from the source at Sumatra towards the west coast of Malaysia and Thailand. Also the computed water levels along the coastal belt appear to be quite reasonable and consistent with the run-up height and estimated water level data. Our study also shows that the nature of the tsunami source has an important influence on whether there will be withdrawal of water from the coastal belt prior to the arrival of the tsunami surge. A regional Cartesian coordinate model is found to be suitable for study different aspects of tsunami along the west coast of Malaysia and Thailand.

Acknowledgements. This research is supported by a short-term grant of Universiti Sains Malaysia and the authors acknowledge the support of the USM short-term grant. The first author wishes to thank the USM authority for allowing him to work as a visiting faculty in the School of Mathematical Sciences. The authors would like to thank Prof S. B. Yoon, Hanyang University, Korea for providing the survey data on the tsunami run-up height along the coastal belt of Penang Island.

References

[1] I. K. Cuypers. *Breakwater Stability Under Tsunami Attack for a site in Nicaragua.* M. Sc. Thesis, Delft University of Technology, The Hague, The Netherlands, 2004.

[2] Imamura, F., Gica, E. C., Numerical Model for Tsunami Generation due to Subaqueous Landslide Along a Coast -A case study of the 1992 Flores tsunami, Indonesia, *Sc. Tsunami Hazards*, 14(1), 1996, 13 - 28.

[3] Johns, B., Rao, A. D., Dube, S. K., Sinha P. C., Numerical modeling of tide surges interaction in the Bay of Bengal, *Phil. Trans. R. Soc. of London*, A313, 1985, 507-535.

[4] Kienle, J.,Kowalik, Z., Troshina, Elen, Propagation and Runup of Tsunami Waves Generated by Mt. St. Augustine Volcano, Alaska, *Sc. Tsunami Hazards*, 14(3), 1996,191-206.

[5] Kowalik, Z., Whitmore, P. M., 1991. An Investigation of Two Tsunamis Recorded at Adak, Alaska. Sc. Tsunami Hazards. 9, 67 - 83.

[6] Kowalik, Z., Knight, W., Whitmore, P. M., 2005. Numerical Modeling of the Tsunami Indonesian Tsunami of 26 December 2004. Sc. Tsunami Hazards. 23(1), 40 - 56.

[7] Okada, Y., Surface Deformation due to Shear and Tensile Faults in a Half Space, *Bull, Seism. Soc. Am.*, 75, 1985, 1135 - 1154.

[8] Roy, G.D., Estimation of expected maximum possible water level along the Meghna estuary using a tide and surge interaction model, *Environment International*, 21(5), 1995, 671-677.

[9] F. P. Shepard. *Submarine Geology*. Harper and Row, NY, 1963.

[10] C. Synolaksis. Tsunami and Seiche. In W. F. Chen and C. Scawthorn, editors, *The Earthquake Engineering Handbook*, pages 9.1 - 9.89. CRS Press, Boca Raton, 2003.

[11] V. V. Titov, F. I. Gonzalez. *Implementation and Testing of the Method of Splitting Tsunami (MOST) Model.* NOAA Technical Memorandum ERL, PMEL - 112, Contribution No. 1927 from NOAA/Pacific Marine Environmental Laboratory, pp 11, 1997.

[12] Zahibo, N., Pelinovsky, E., Kurkin, A., Kozelkov, A., Estimation of Far-Field Tsunami Potential for the Caribbean Coast Based on Numerical Simulation, *Sc. Tsunami Hazards*, 21(4), 2003, 202 - 222.